

Simulated precipitation diurnal cycles over East Asia using different CAPE-based convective closure schemes in WRF model

Ben Yang^{1,2} · Yang Zhou^{1,2}  · Yaocun Zhang^{1,2} · Anning Huang^{1,2} · Yun Qian³ · Lujun Zhang^{1,2}

Received: 11 January 2017 / Accepted: 25 April 2017 / Published online: 5 May 2017
© Springer-Verlag Berlin Heidelberg 2017

Abstract Closure assumption in convection parameterization is critical for reasonably modeling the precipitation diurnal variation in climate models. This study evaluates the precipitation diurnal cycles over East Asia during the summer of 2008 simulated with three convective available potential energy (CAPE) based closure assumptions, i.e. CAPE-relaxing (CR), quasi-equilibrium (QE), and free-troposphere QE (FTQE) and investigates the impacts of planetary boundary layer (PBL) mixing, advection, and radiation on the simulation by using the weather research and forecasting model. The sensitivity of precipitation diurnal cycle to PBL vertical resolution is also examined. Results show that the precipitation diurnal cycles simulated with different closures all exhibit large biases over land and the simulation with FTQE closure agrees best with observation. In the simulation with QE closure, the intensified PBL mixing after sunrise is responsible for the late-morning peak of convective precipitation, while in the simulation with FTQE closure, convective precipitation is mainly controlled by advection cooling. The relative contributions of different processes to precipitation formation are functions of rainfall intensity. In the simulation with CR closure, the dynamical equilibrium in the free troposphere still can be reached, implying the complex cause-effect relationship between atmospheric motion and convection. For

simulations in which total CAPE is consumed for the closures, daytime precipitation decreases with increased PBL resolution because thinner model layer produces lower convection starting layer, leading to stronger downdraft cooling and CAPE consumption. The sensitivity of the diurnal peak time of precipitation to closure assumption can also be modulated by changes in PBL vertical resolution. The results of this study help us better understand the impacts of various processes on the precipitation diurnal cycle simulation.

Keywords Precipitation diurnal cycle simulation · Convective closure · Boundary-layer resolution · East Asia · WRF model

1 Introduction

The diurnal cycle of precipitation is a pronounced climatological phenomenon closely associated with the diurnal evolutions of near-surface properties and upper-layer large-scale forcing (e.g. Donner and Phillips 2003; Dai and Trenberth 2004; Bechtold et al. 2014; Wu et al. 2015). The precipitation diurnal variation can have large impacts on surface hydrology such as evaporation and runoff and thus surface temperature (Dai 1999). Currently, accurate modeling of the precipitation diurnal cycle, especially over land, remains a big challenge for the climate community. In fact, even models with sophisticated physics parameterizations still have difficulties in reproducing the diurnal variation of precipitation (e.g. Dai and Trenberth 2004; Yuan 2013) because the generation of precipitation is controlled by many coupled processes among the planetary boundary layer (PBL), cumulus convection, cloud microphysics, and so on (e.g. Leung et al. 1999; Arakawa 2004; Cha et al.

✉ Yang Zhou
yangzhou@nju.edu.cn

¹ CMA-NJU Joint Laboratory for Climate Prediction Studies, Institute for Climate and Global Change Research, School of Atmospheric Sciences, Nanjing University, Nanjing, China

² Collaborative Innovation Center of Climate Change, Nanjing, Jiangsu, China

³ Pacific Northwest National Laboratory, Richland, WA, USA

2008; Yang et al. 2012, 2015a; Qiao and Liang 2016). As a result, evaluation of the simulated precipitation diurnal cycle has useful implications not only for the improvement in precipitation prediction but also for the validation of model physics parameterizations (e.g. Suhas and Zhang 2015).

Over East Asia, summer precipitation is featured by remarkable diurnal variation that varies from region to region because of the spatial heterogeneity in terrain and underlying surface type (Qian and Leung 2007; Yu et al. 2007; Zhou et al. 2008; He and Zhang 2010). It is found, that precipitation amount generally peaks in late afternoon over most areas of southern China (SC) and northeastern China (NEC), and at midnight over southwestern China (Li et al. 2008; Chen et al. 2016). Differently, precipitation over central eastern China is featured by two comparable peaks in late afternoon and early morning, which respectively result from the late-afternoon peak in convective precipitation and the early-morning peak in stratiform precipitation (Yuan et al. 2013). Zhou et al. (2008) compared two satellite products of precipitation with rain-gauge records and concluded that the diurnal cycles of precipitation intensity and frequency are similar to those of precipitation amount for most regions in China except for the Yangtze River valley (YRV).

Many previous studies have investigated the performance of climate models in simulating the precipitation diurnal cycle including that over East Asia (e.g. Dai and Trenberth 2004; Yuan 2013). Among different model physics, convection parameterization scheme (CPS) has been found to be the main source of error in the simulated precipitation diurnal variation, and the skills of different CPSs are highly regime dependent (Liang et al. 2004; Yuan 2013; Qiao and Liang 2016). Dai and Trenberth (2004) showed that in version 2 of the community climate system model, convection occurs too early over land when compared with observation. By applying the weather research and forecasting (WRF) model, Jin et al. (2016) revealed that the diurnal phase of convective precipitation over East Asia is not sensitive to horizontal resolution but exhibits large response to the modifications of CPSs. Zhang and Chen (2016) evaluated the results of the superparameterized CAM5 (i.e. the community atmospheric model version 5) and the standard CAM5 that applies the Zhang–McFarlane (ZM) CPS, showing that the latter is unable to reproduce the different stages of convection and produces a too early peak in precipitation over continental East Asia. Qiao and Liang (2015) found that the Grell scheme (Grell 1993) performs better in simulating the precipitation diurnal cycle over the Central United States compared to other CPSs.

In CPSs, closure assumption is the most fundamental component as it determines the intensity of convection for each model grid point at each time (Yano et al. 2013;

Zhang 2002; Wu 2012; Suhas and Zhang 2015). Yuan (2013) attributed the biases in the precipitation diurnal cycle over China in different AMIP5 (i.e. atmospheric model intercomparison project phase 5) models to the CPSs, in which the convective closures largely control the precipitation diurnal cycle. The convective closure is usually dependent on the convective available potential energy (CAPE) (Arakawa and Schubert 1974; Kain and Fritsch 1993; Zhang and McFarlane 1995), environmental upward vertical velocity (Brown 1979; Frank and Cohen 1987), or moisture advection or convergence (Krishnamurti et al. 1983). A review by Yano et al. (2013) suggested that the low-to-middle troposphere moisture is important for convective intensity when CAPE is small, but becomes less important when large CAPE variation exists. However, they also pointed out that it is more nature to take an energy (e.g. CAPE) cycle of convection as the base for closure. Convective instability or CAPE can be affected by both fast-varying processes in the PBL and large-scale forcing in the free troposphere. Arakawa and Schubert (1974) introduced the quasi-equilibrium (QE) concept that the convection-induced stabilization and the destabilization by non-convective processes in the whole atmospheric column are in balance. Raymond (1995) and Emanuel (1995) proposed a different version of QE, in which an equilibrium is sustained between surface fluxes and convective downdrafts in the PBL. Observational analysis by Zhang (2002), however, showed that the contribution of PBL fluxes to CAPE change is much larger than that by convection at subdiurnal timescales in midlatitudes. Thus, he proposed a modified QE assumption, i.e. CAPE change by convective and large-scale processes in the free troposphere above the PBL are in balance. However, he also pointed out that the PBL forcing is still important given that the PBL is the source layer of convective updraft and the sink of convective downdraft. To better represent the precipitation diurnal variation in large-scale models, Bechtold et al. (2014) developed a new CAPE-type closure based on the QE assumption for the free troposphere but with the boundary forcing also considered. With the new closure, the precipitation diurnal phases over the continental United States and Africa are significantly improved.

Previous studies about the convective closure impacts on the precipitation diurnal cycle simulation over East Asia were mainly conducted using different models with various differences in model physics and dynamical configurations such as horizontal and vertical resolutions. The purpose of this study is to evaluate and compare the simulated diurnal cycles over East Asia with three different CAPE-based closures in the ZM CPS in WRF. Here, WRF is reinitiated every day so as to isolate the impacts of convective closure from that potentially induced by drifts in large-scale circulations. We also intend to investigate the

relative contributions of different atmospheric processes (i.e. advection, radiation, and PBL processes) to the precipitation diurnal cycles simulated with different closures. In addition, given the importance of PBL forcing on convection properties (e.g. Zhang 2002; Donner and Phillips 2003; Dai and Trenberth 2004), model vertical configuration, particularly in the PBL, is expected to have large impacts on the diurnal evolution of the convective source layer properties and downdraft cooling effect. Therefore, we also explore the potential impacts of the PBL vertical resolution on the precipitation diurnal cycles simulated by different closures.

The paper is organized as follows: Sect. 2 describes the applied convective closures, WRF model configurations, and datasets. In Sect. 3 we evaluate the simulated precipitation diurnal cycles over East Asia with different closures and analyze the relative contributions of the PBL and free-troposphere processes to the precipitation formation. The impacts of vertical resolution in the PBL on the simulated precipitation and their underlying mechanisms are also explored. A summary of the main findings is given in Sect. 4.

2 Model experiments, dataset, and methods

2.1 Convective closure

CAPE is a physical measure of convective instability (Yano et al. 2013), which is defined as the vertical integral of the difference in virtual temperature (i.e. buoyancy) between the air parcel and the environment as the parcel is lifted from its source layer to the level of neutral buoyancy. In the ZM CPS, the lifted parcel is diluted by its environmental air, which is introduced by Neale et al. (2008).

Following the convention in Zhang (2002), the net change in CAPE is the sum of changes induced by convective processes and by large-scale processes (denoted by subscripts *cu* and *ls*, respectively):

$$\frac{\partial \text{CAPE}}{\partial t} = \left(\frac{\partial \text{CAPE}}{\partial t}\right)_{cu} + \left(\frac{\partial \text{CAPE}}{\partial t}\right)_{ls}. \tag{1}$$

Also, CAPE change can be written as the sum of changes due to virtual temperature tendencies of the air parcel and its environment (denoted by subscripts *p* and *e*, respectively):

$$\frac{\partial \text{CAPE}}{\partial t} = \frac{\partial \text{CAPE}_p}{\partial t} + \frac{\partial \text{CAPE}_e}{\partial t}. \tag{2}$$

The first term on the right hand is generally determined by changes in the PBL properties, while the second term is mainly controlled by virtual temperature changes in the

free troposphere induced by convection and large-scale forcing such as advection and radiative processes.

Because convective and large-scale processes can affect both the thermal properties of the air parcel and its environment, the net change in total CAPE can further be broken into four components:

$$\begin{aligned} \frac{\partial \text{CAPE}}{\partial t} = & \left(\frac{\partial \text{CAPE}_p}{\partial t}\right)_{cu} + \left(\frac{\partial \text{CAPE}_p}{\partial t}\right)_{ls} + \left(\frac{\partial \text{CAPE}_e}{\partial t}\right)_{cu} \\ & + \left(\frac{\partial \text{CAPE}_e}{\partial t}\right)_{ls}. \end{aligned} \tag{3}$$

The four components are contributed by (1) change of PBL virtual temperature from convective processes, (2) change of PBL virtual temperature from large-scale processes, (3) change of free-troposphere virtual temperature from convective processes, and (4) change of free-troposphere virtual temperature from large-scale processes.

In the below, we briefly introduce the three different CAPE-based closures based on the concepts of CAPE-relaxing (CR), QE, and free-troposphere QE (FTQE).

In the QE assumption, CAPE change induced by convective processes and that by non-convective processes are in balance:

$$\left(\frac{\partial \text{CAPE}}{\partial t}\right)_{cu} = -\left(\frac{\partial \text{CAPE}}{\partial t}\right)_{ls}. \tag{4}$$

Based on field observations derived from the atmospheric radiation measurement, Zhang (2002) proposed the FTQE assumption, in which CAPE change by convective and large-scale processes in the free troposphere above the PBL are in balance:

$$\left(\frac{\partial \text{CAPE}_e}{\partial t}\right)_{cu} = -\left(\frac{\partial \text{CAPE}_e}{\partial t}\right)_{ls}. \tag{5}$$

Another common CAPE-type closure is based on the CR concept, in which the total CAPE is relaxed to a reference value (i.e. CAPE_0) over a specified time τ (e.g. Kain and Fritsch 1993; Zhang and McFarlane 1995):

$$\left(\frac{\partial \text{CAPE}}{\partial t}\right)_{cu} = -\frac{\text{CAPE} - \text{CAPE}_0}{\tau}. \tag{6}$$

2.2 Model and experiments

The advanced research WRF model version 3.7.1 (Skamarock et al. 2008) is used. All the WRF experiments apply the ZM CPS (Zhang and McFarlane 1995), which is adopted from the CAM5 physics (Ma et al. 2014) and is the basis for the CPSs in many other general circulation models (GCMs) (e.g. Wu et al. 2010; Bao et al. 2013; Ji et al. 2014). The CR closure is the standard configuration

in the ZM CPS in WRF3.7.1 (Zhang and McFarlane 1995; Ma et al. 2014). We also incorporate the QE and FTQE closures into the ZM CPS. Here, CAPE tendency by non-convective processes is calculated as the sum of CAPE change induced by advection, radiation, and PBL processes. The contribution of each process is also diagnosed.

Different closures are generally tied with different trigger functions for convection, which can have large impacts on the simulated precipitation diurnal cycle (e.g. Suhas and Zhang 2014). In this study, the corresponded trigger function for the CR closure is:

$$CAPE > CAPE_0. \tag{7}$$

Here, $CAPE_0$ is set as the default value of 70 J kg^{-1} in the ZM CPS in WRF (Ma et al. 2014). We also need to specify the value of τ (in Eq. 6), a time scale during which the total CAPE is relaxed to $CAPE_0$ by convection. Previous sensitivity studies (e.g. Yang et al. 2013) showed that τ is a key parameter for the precipitation simulation in CAM5. Following the definition in WRF, τ is set as a function of horizontal grid spacing Δx :

$$\tau = \max(\tau_{\min}, \tau_{\max} \cdot \frac{\Delta x}{\Delta x_0}), \tag{8}$$

where $\tau_{\min} = 600 \text{ s}$, $\tau_{\max} = 3600 \text{ s}$, and $\Delta x_0 = 275 \text{ km}$. With this formula, the ZM CPS can remove CAPE quickly enough in fine-resolution simulations.

For the QE (FTQE) closure, convection is activated when there exists a positive CAPE tendency induced by large-scale processes in the whole atmospheric column (in the free troposphere).

Many other trigger functions have been tested by previous studies. For example, Lee et al. (2008) revealed that the distance from cloud base to convection starting level

(CSL) must be less than 150 hPa, so as to realistically simulate the nocturnal rain over the US Great Plains. In Wu scheme (Wu 2012), convection can only be activated when the CSL air is sufficiently moist, i.e., the relative humidity (RH) at CSL is above 70%. Given that the impacts of convective closure on precipitation could be modulated by using different convection triggers, for each closure we conduct two experiments with the RH restriction (as in Wu scheme) off and on in the trigger function. Besides the above experiments, we also conduct an additional simulation in which convection is entirely prohibited to aid the analysis.

Different vertical resolutions in the PBL are configured to explore the potential impacts of vertical resolution on the precipitation diurnal cycle. In the low-resolution experiments, there are 34 layers from the surface to 50 hPa with about five layers in the lowest 200 m and ten layers in 200–2000 m. Two high-resolution experiments are conducted, respectively with five additional vertical layers in 0–200 and 200–2000 m above the surface against the low-resolution experiments. More details about the experimental configurations are listed in Table 1.

The model domain (Fig. 1) covers most parts of the Asian summer monsoon region and encompasses approximate $10^\circ\text{--}55^\circ\text{N}$ and $75^\circ\text{--}165^\circ\text{E}$, with a horizontal grid spacing of 100 km. A relatively low horizontal resolution is used because the ZM CPS is primarily developed for GCMs that are usually run at resolutions of $1^\circ\text{--}2^\circ$. Meteorological fields such as temperature, water vapor, and geopotential height used for generating the initial and boundary conditions are provided by the National Centers for Environmental Prediction (NCEP) operational global final (FNL) analyses with a $1^\circ \times 1^\circ$ grid spacing and 6-h interval (<http://rda.ucar.edu/datasets/ds083.2/>).

Table 1 A list of experiments and corresponded convective closures, trigger functions, and vertical resolutions in the PBL

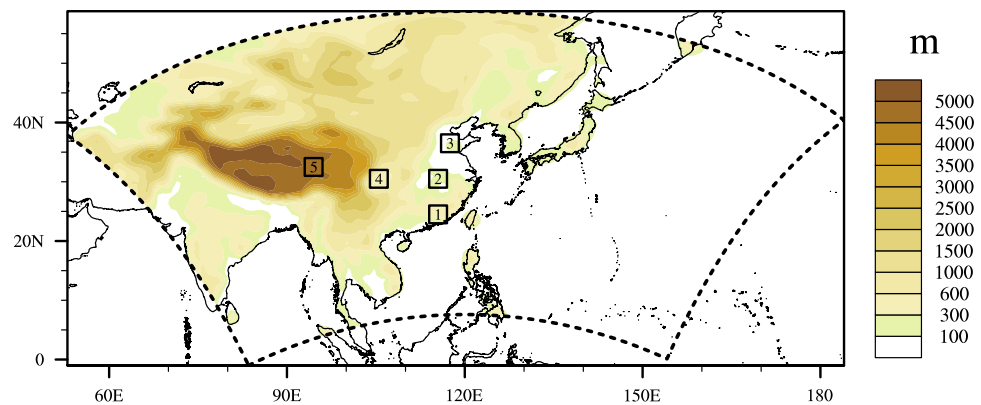
Experiments	Closure assumption	With RH restriction in trigger function?	PBL vertical resolution
CR	CR assumption ^a	No	Low
CR_H200/CR_H2000	CR assumption	No	High in 0–200/200–2000 m
CR_RH	CR assumption	Yes	Low
QE	QE assumption ^b	No	Low
QE_H200/QE_H2000	QE assumption	No	High in 0–200/200–2000 m
QE_RH	QE assumption	Yes	Low
FTQE	FTQE assumption ^c	No	Low
FTQE_H200/FTQE_H2000	FTQE assumption	No	High in 0–200/200–2000 m
FTQE_RH	FTQE assumption	Yes	Low
NONE	–	–	Low
NONE_H200	–	–	High in 0–200 m

^aCorresponded trigger function: $CAPE > 70 \text{ J Kg}^{-1}$

^bCorresponded trigger function: $CAPE > 0 \text{ J Kg}^{-1}$ and $\left(\frac{\partial CAPE}{\partial t}\right)_{ls} > 0$

^cCorresponded trigger function: $CAPE > 0 \text{ J Kg}^{-1}$ and $\left(\frac{\partial CAPE_c}{\partial t}\right)_{ls} > 0$

Fig. 1 WRF Model domain (dashed boxes) with grid spacing of 100 km. Solid boxes denote the 5 sub-regions of 1 southeastern Southern China (SC), 2 middle Yangtze River valley (YRV), 3 Northern China plain (NCP), 4 Sichuan Basin (SCB), and 5 central Tibet Plateau (TP). Shades indicate the terrain



Sea surface temperature is also prescribed from the FNL analysis and updated every 6 h.

In WRF, the ZM CPS can only be used with two PBL schemes, i.e. the Mellor–Yamada–Janjić (MYJ, Janjić 2002) scheme and the University of Washington (UW, Bretherton and Park 2009) scheme. Test experiments showed that WRF always crashes with the UW PBL scheme when a very high vertical resolution in the PBL is used. As a result, the MYJ PBL scheme is used in this study. Other model physics packages applied here include the UW shallow convection scheme (Park and Bretherton 2009), the Morrison 2-Moment microphysics scheme (Morrison et al. 2005), the radiation scheme of the rapid radiative transfer model for general circulation models (Barker et al. 2003; Pincus et al. 2003), the Noah Land Surface Model (Chen and Dudhia 2001), and the Eta surface layer scheme (Janjić 1994, 2002).

Dai (1999) pointed out that the interannual variability in the diurnal cycle of summer precipitation over the contiguous United States is small. The same situation is found over East Asia (see Sect. 3.2). Therefore, all experiments are conducted for only one summer, i.e. 1 June to 31 August 2008. Because of the fast increasing of the simulation errors in large-scale circulation, all experiments are reinitialized every day following Yang et al. (2012). Here, for each day from 1 June to 31 August 2008, WRF is integrated for 36 h, with the first 12 h discarded as model spin-up and the results of the last 24 h of each day concatenated as a continuous time series. This strategy helps to minimize the differences in large-scale circulations among different experiments and better reflect the responses of the precipitation diurnal cycle simulation to the changes in convective closure.

2.3 Dataset

Satellite-retrieved precipitation products from the Global Precipitation Climatology Project (GPCP, available at <http://www1.ncdc.noaa.gov/pub/data/gpcp/1dd-v1.2>;

Huffman et al. 2001) and Tropical Rainfall Measuring Mission (TRMM, Huffman et al. 2007) for the period of 1 June to 31 August 2008 are used. GPCP precipitation (1°, daily) is derived from multiple satellite-retrieved products and has been verified against surface rain-gauge records. Precipitation products from TRMM 3B42 version 7 (referred to as TRMM3B42; available at <ftp://disc2.nascom.nasa.gov/data/TRMM/Gridded>; Huffman et al. 2007; Huang et al. 2016) with a spatial resolution of 0.25° and a temporal resolution of 3 h are applied to evaluate the simulated precipitation diurnal cycle. In addition to the satellite precipitation products, we also use the hourly data from station rain gauges, which is acquired from the National Meteorological Information Center of China Meteorological Administration.

Rainfall events detected by TRMM precipitation radar (PR) can be classified into different precipitation types, e.g., convective and stratiform precipitation, based on the horizontal and vertical variability and maximum values of the observed radar reflectivity (Kozu et al. 2001; Schumacher and Houze 2003; Yang et al. 2013). The TRMM convective precipitation and model convective precipitation share many common features despite of some inconsistencies between them. In mass-flux type CPSs including the ZM scheme, precipitation is generated once the convective updrafts can penetrate through the unstable layers to a certain height (Zhang and McFarlane 1995; Kain 2004). Thus, CPSs tend to parameterize the unresolved component of the moist convective process (Arakawa 2004) and the simulated precipitation and associated condensation heating profiles can be taken into account as convective type. Actually, the TRMM convective precipitation has been used for model evaluation and calibration in previous studies (e.g. Yuan 2013; Yang et al. 2013). So we believe that the simulated convective precipitation, especially at relatively coarse resolution as in this study, is in accordance with our understanding about the definition of convective precipitation in the real atmosphere. Here, we use the TRMM PR 2A25 (referred to as TRMM2A25) dataset (37°S–37°N; available at <http://disc.sci.gsfc.nasa.gov/precipitation/>

[documentation/TRMM_README/TRMM_2A25_readme.shtml/](#)) to obtain the diurnal variation of convective precipitation. Although different precipitation datasets are used, this study mainly focuses on the comparison of the convective precipitation simulated by different convective closures.

2.4 Analysis method

Satellite-retrieved and station rain-gauge precipitation products are first regridded onto the model grid points. Following Zhou et al. (2008), precipitation frequency is calculated as the percentage of all hours in the summer of 2008 having measurable precipitation for each grid box and each hour. In this study, measurable precipitation is defined as $>0.1 \text{ mm h}^{-1}$ that is the minimum precipitation amount recorded in the rain-gauge data. Precipitation intensity is computed as the mean rates averaged during the precipitating hours. Rainy events for each hour are further classified into five categories based on their hourly rainfall amounts, i.e. none-rain ($<0.1 \text{ mm h}^{-1}$), light-rain ($0.1\text{--}2.5 \text{ mm h}^{-1}$), moderate-rain ($2.5\text{--}7.6 \text{ mm h}^{-1}$), and heavy-rain ($>7.6 \text{ mm h}^{-1}$) events, which are following the definitions in the website of <https://en.wikipedia.org/wiki/Rain#Intensity>.

3 Results

3.1 Spatial distribution of precipitation amount

The total precipitation amounts during the summer of 2008 simulated with different convective closures are evaluated against GPCP and TRMM3B42 products (Fig. 2). Overall, the precipitation from the two satellite products (Fig. 2a, b) are comparable in terms of magnitude and spatial pattern, except that the precipitation amount in TRMM3B42 is a little larger than that in GPCP. In observation, rainfall centers with large precipitation amount can be found over the Bay of Bengal, the South China Sea, and their coastal areas. There is a rain band extending from eastern China to Japan. A separate rain band can also be detected in the ocean areas to the east of Japan. Because large-scale circulation and temperature fields were reinitiated every day, the simulations with different closures all reasonably reproduce the spatial distribution of precipitation as that in observation. However, large differences in the magnitudes of the simulated precipitation are found among different experiments. In the CR experiment in which the CR closure is used (Fig. 2c), precipitation magnitude is underestimated over most land and ocean regions compared to observations. Among all the experiments, the QE experiment simulates the largest precipitation amount, with apparent

overestimation of precipitation over ocean areas, particularly over the southern and eastern lateral boundary areas of model domain. Compared to the CR experiment, the precipitation amount in the FTQE experiment is relatively larger over oceans. When the RH restriction (i.e. $\text{RH} > 70\%$ at CSL) is considered in the trigger function, the simulated precipitation amounts are reduced for all the experiments with different closures; however, the changes by using different trigger functions are not as large as those induced by using different convective closures.

3.2 Precipitation diurnal cycle

The simulated precipitation diurnal variations are further evaluated. The spatial distributions of summertime precipitation diurnal phases, in terms of amount, frequency, and intensity (see Sect. 2.4) in TRMM3B42 and rain-gauge data are shown in Fig. 3. The results show that the precipitation diurnal features vary from region to region. For each observation, i.e. TRMM3B42 or rain-gauge data, the results in 2008 are overall similar to that averaged in 2008–2010, indicating that the year-to-year variation in precipitation diurnal phases is small, similar to the condition over the contiguous United States (Dai 1999). In TRMM3B42, precipitation amount over most land areas (Fig. 3a, d) peaks from late afternoon to early evening (indicated by hue in Fig. 3) except for over the Sichuan Basin (SCB, see Fig. 1 for locations) and the southern side of TP, consistent with what have been found by previous studies (e.g. Yu 2007; Li et al. 2008; Zhou et al. 2008; Chen et al. 2016). For most parts of SCB, precipitation amount peaks at midnight or early morning. For ocean regions, precipitation amount generally peaks at early morning. Similar to the results based on precipitation amount, precipitation frequency generally peaks from noon to late afternoon except for over SCB (Fig. 3b, e). Compared to precipitation frequency, apparent midnight peaks of precipitation intensity (Fig. 3c, f) can be found over northern China plain (NCP), YRV, and SCB.

In the rain-gauge data, precipitation amount (Fig. 3g, j) peaks at afternoon over SC, midnight over SCB, and late afternoon to early evening over TP, which is quite similar to the TRMM3B42 results. Over YRV and NCP, however, the midnight or early-morning peaks are more obvious in rain-gauge data than in TRMM3B42 because of the deficiency of the satellite products in detecting the morning peak of precipitation (Zhou et al. 2008). The spatial distributions of precipitation frequency and intensity based on the rain-gauge data is generally consistent with the TRMM3B42 results.

The spatial distributions of precipitation diurnal phases during the summer of 2008 simulated with different closures are compared in Fig. 4. Apparent differences in

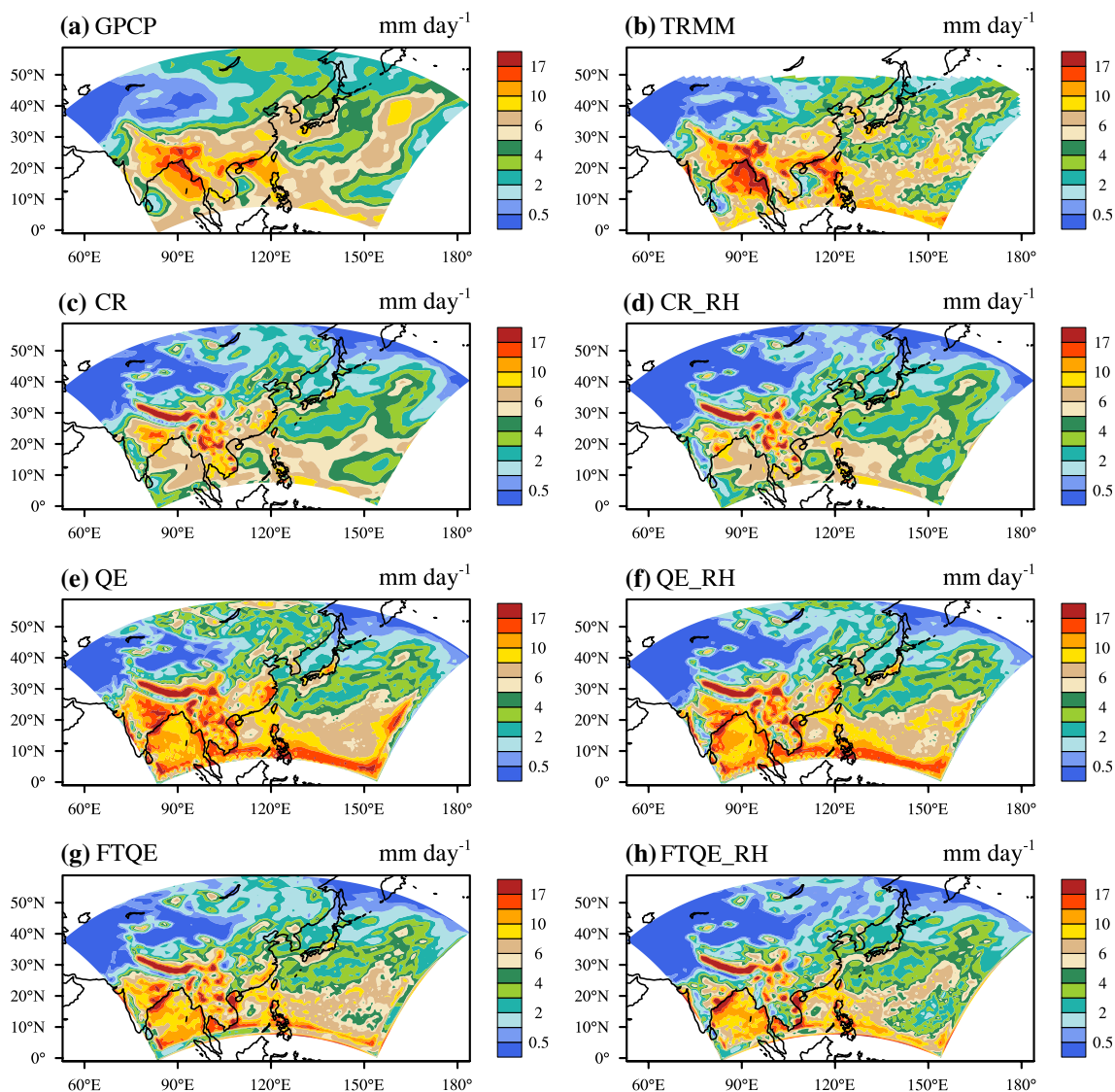


Fig. 2 Spatial distribution of total precipitation in the summer of 2008 from GPCP (a), TRMM3B42 (b), and the CR (c), CR_RH (d), QE (e), QE_RH (f), FTQE (g), and FTQE_RH (h) simulations

the peak time of precipitation are found among different experiments. In the CR experiment (Fig. 4a), precipitation amount peaks at around late afternoon over TP and Indochina. Remarkable south-to-north difference in the diurnal phase of precipitation amount can be found in eastern China (20°–40°N and 113°–122°E). Precipitation amount reaches its maximum at afternoon in SC, while at noon in YRV. Precipitation amount in NEC (40°–46°N and 118°–130°E) is mostly featured by a noon-time peak. Different from precipitation amount, precipitation frequency (Fig. 4b) in the CR experiment is featured by late-afternoon peaks over SC, NEC, and TP and noon peaks over YRV and NCP. By contrast, precipitation intensity peaks at midnight or early morning for most parts of China.

In the QE experiment, precipitation amount over land (Fig. 4d) generally peaks from late morning to noon with

large diurnal variation amplitude (indicated by saturation in Fig. 4). The spatial distribution of precipitation amount is similar to that of precipitation frequency and intensity (Fig. 4e, f).

In the FTQE experiment, precipitation amount peaks from late afternoon to early evening (green color in Fig. 4g) for most land regions; this is mainly because of the large precipitation frequency at around 2000LST (Fig. 4h). In NCP and SCB, diurnal peaks of precipitation amount can be found at midnight or early morning as observed, which is mainly due to the large precipitation intensity during nighttime (Fig. 4i).

In all the experiments, precipitation amount generally peaks at early morning over oceans, particularly over the near-land areas. However, the inter-simulation differences in precipitation diurnal phases are more apparent over land

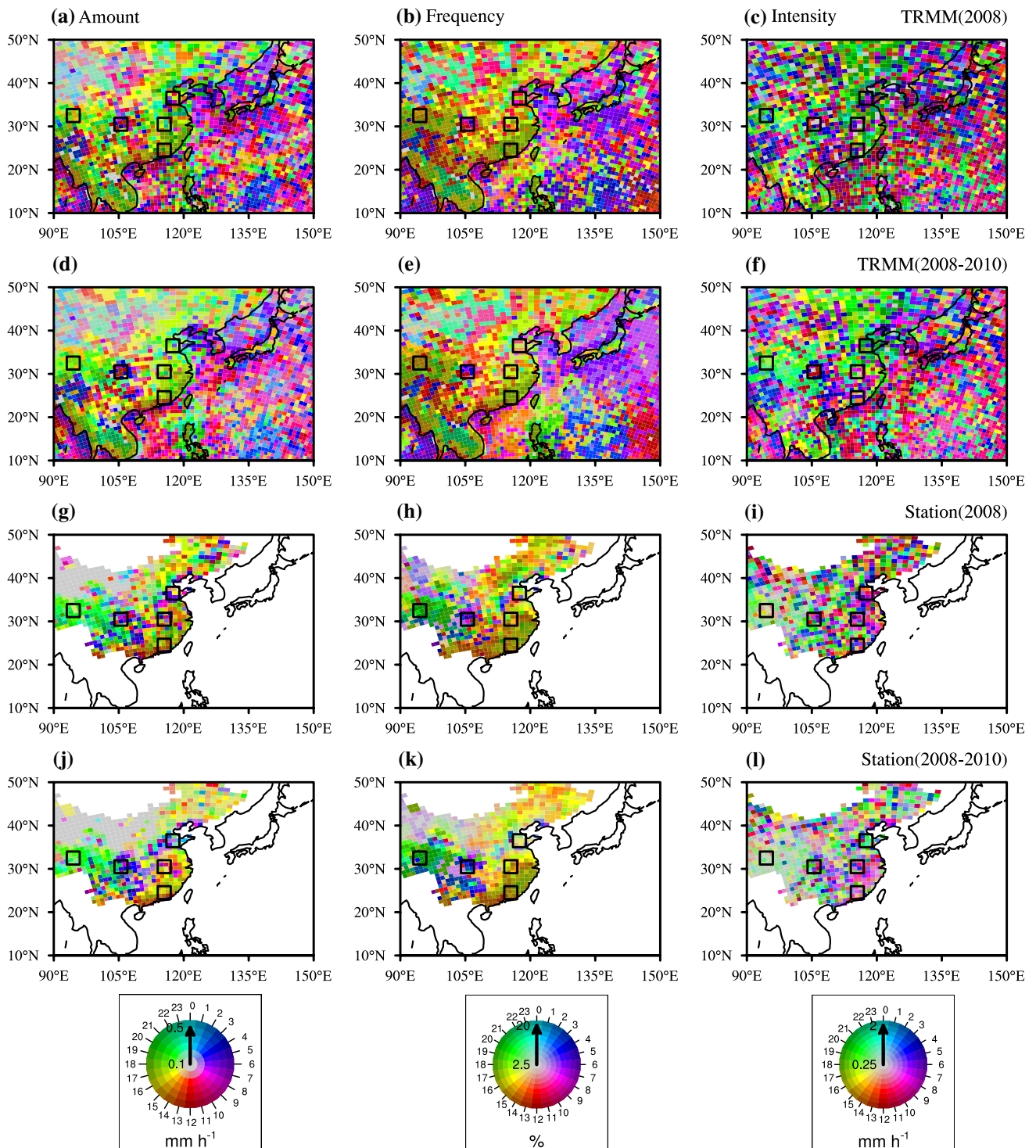


Fig. 3 Spatial distribution of diurnal peak time (LST Time; indicated by hue) and diurnal variation amplitude (indicated by saturation) for summertime total precipitation amount (*left*), frequency (*center*), and

intensity (*right*) in TRMM3B42 (a–c 2008, d–f 2008–2010) and in station rain-gauge data (g–i 2008, j–l 2008–2010)

than over ocean regions. The CR and QE experiments fail to reproduce the diurnal variation of precipitation over land shown in observations (Fig. 3). Contrastingly, the FTQE experiment shows better agreements with observations in

terms of precipitation amount, which is overall consistent with previous findings based on the results over China and over the United States (Yuan 2013; Qiao and Liang 2015, 2016).

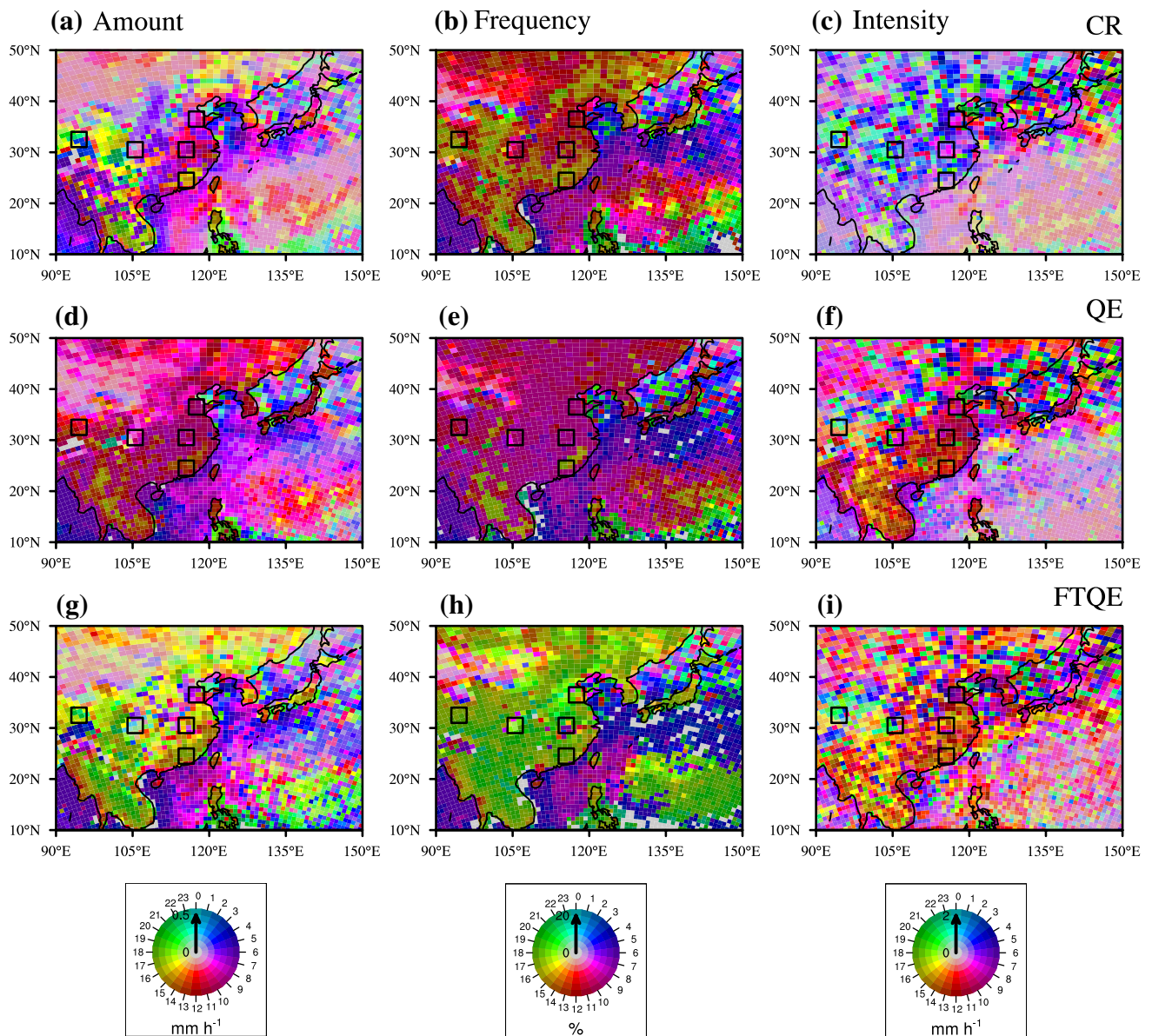


Fig. 4 Spatial distribution of diurnal peak time (LST Time; indicated by hue) and diurnal variation amplitude (indicated by saturation) for total precipitation amount (*left*), frequency (*center*), and inten-

sity (*right*) in the summer of 2008 from the CR (a–c), QE (d–f), and FTQE (g–i) simulations

In Fig. 5 we also evaluate the simulated precipitation diurnal cycles (normalized values) against observations at five sub-regions (see Fig. 1) with different precipitation characteristics (e.g. Zhou et al. 2008; Chen et al. 2016). In observations (black curves and dots in Fig. 5), precipitation amount peaks at afternoon over southern SC (Fig. 5a). Over middle YRV (Fig. 5d) and NCP (Fig. 5g), precipitation amount is featured by two peaks, one at afternoon and the other one in the early morning. Precipitation amount peaks at midnight over SCB (Fig. 5j) and early evening over central TP (Fig. 5m). For most regions, the afternoon peaks of precipitation amount in

observations are generally because of the high precipitation frequency at afternoon (center column in Fig. 5), while the midnight peaks are due to the large precipitation intensity at night (right column in Fig. 5). The high occurring frequency of nighttime precipitation over SCB (Fig. 5k) also contributes to the nighttime peak of precipitation amount there (Fig. 5j).

Similar to the results in Fig. 4, the FTQE experiment (green curves in Fig. 5) agrees best with observations in terms of the diurnal cycle of precipitation amount for most sub-regions. However, the performances of different closures in simulating the precipitation frequency and

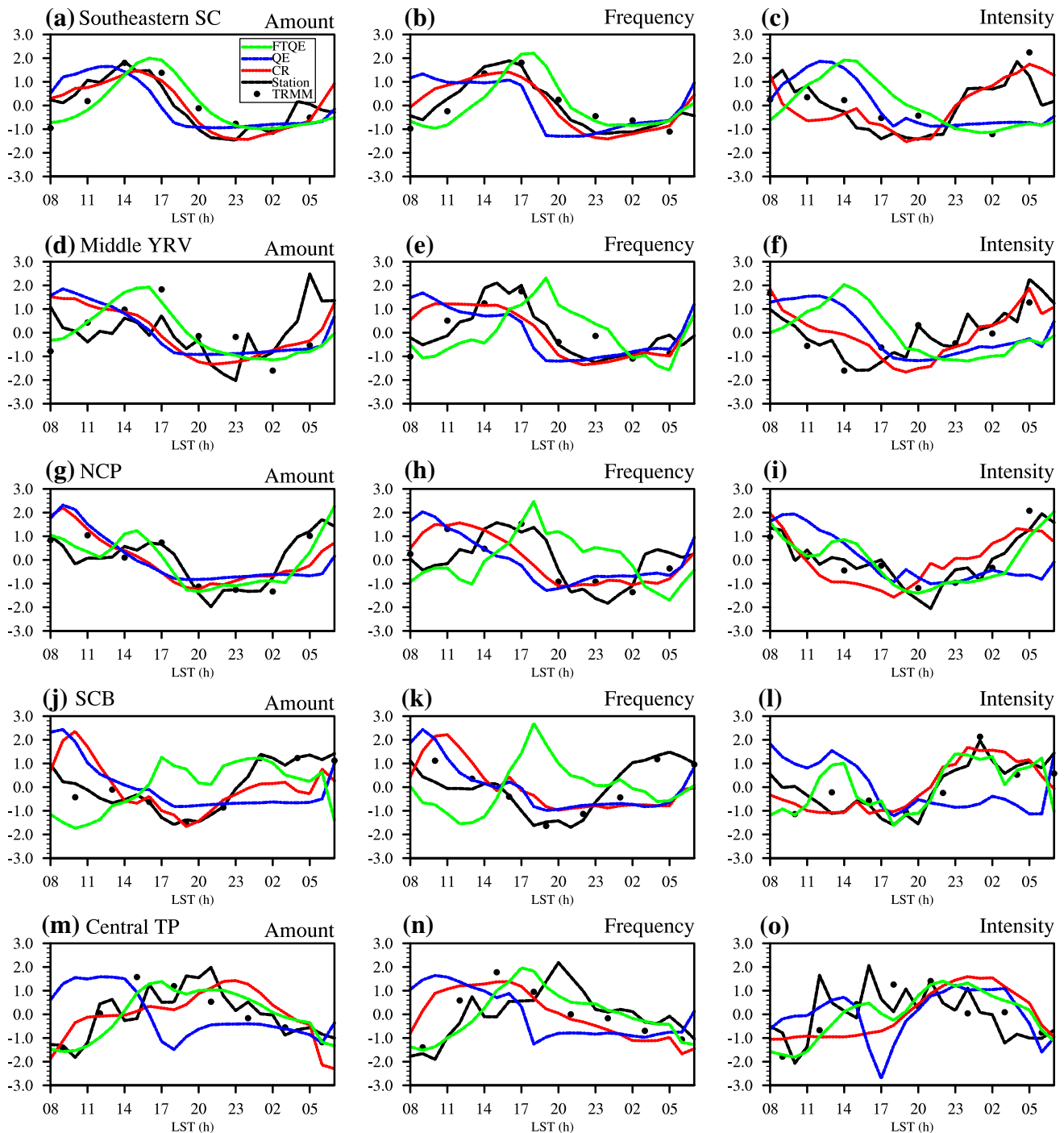


Fig. 5 Diurnal variations (normalized by the daily mean and standard deviation) of precipitation amount (*left*), frequency (*center*), and intensity (*right*) over different sub-regions (see Fig. 1) in the summer

of 2008 from observations of TRMM3B42, station records, and the CR, QE, and FTQE simulations

intensity are dependent on locations, and none of them is superior to others for all the sub-regions.

The diurnal feature of convective precipitation can be different from that of total precipitation. Figure 6 presents the spatial distribution of nighttime (2300–0500 Beijing time) minus daytime (1100–1700 Beijing time)

precipitation amount during the summer of 2008 in observations (TRMM3B42 for total precipitation and TRMM2A25 for convective precipitation) and simulations with different closures. Similar results can be found when nighttime (daytime) is defined as 2000–0700 (0800–1900) Beijing time. It should be noted that nighttime or daytime

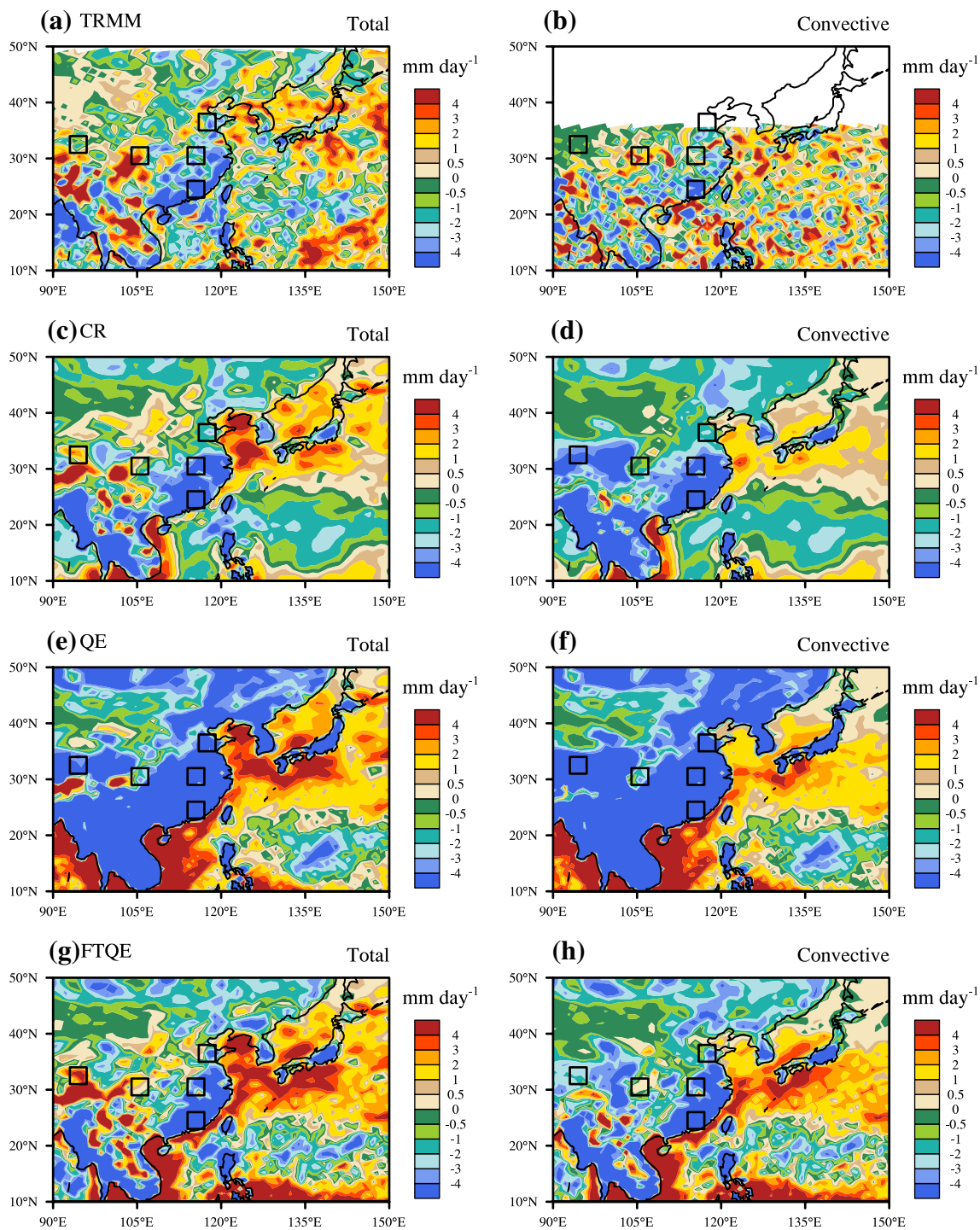


Fig. 6 Nighttime (2300–0500 Beijing time) minus daytime (1100–1700 Beijing time) precipitation amount for total (left) and convective (right) precipitation in the summer of 2008 from TRMM3B42/TRMM2A25 (a, b), and the CR (c, d), QE (e, f), and FTQE (g, h) simulations

here is defined based on Beijing time (rather than LST) so as to simplify the manipulation of TRMM data at 3-h interval. In TRMM3B42, daytime precipitation is larger than nighttime precipitation over SC, while more nighttime precipitation than daytime precipitation is found over SCB

and parts of NCP; these distributions are consistent with the results in Figs. 3a and 5. All the three experiments with different closures (Fig. 6c, e, g) can reproduce the daytime-nighttime difference of precipitation in SC. However, only the CR and FTQE experiments (Fig. 6c, g) can partially

simulate the nocturnal precipitation in SCB and NCP. The distribution of convective precipitation in TRMM2A25 (Fig. 6b) is almost similar to that of total precipitation over land, i.e. more daytime precipitation in SC while more nighttime precipitation over SCB. On the contrary, the results simulated by all the closures are generally featured by negative differences between nighttime and daytime over land, except for some sporadic areas in the CR and FTQE (Fig. 6d, h) experiments. Yuan (2013) revealed that the well simulated precipitation diurnal phases in some models are mainly because of their high performance in simulating the partitioning between convective and stratiform precipitation, rather than the well simulated diurnal variation of convective precipitation. The comparison in Fig. 6 indicates that the nocturnal precipitation over SCB and NCP in the CR and FTQE experiments are mainly contributed by stratiform precipitation from the microphysics scheme. In the QE experiment, by contrast, the ratio of stratiform to total precipitation is very small due to the QE closure producing too much convective precipitation. Because convective precipitation is the main focus of this study, only the diurnal features of convective precipitation during the summer of 2008 are analyzed in the following sections.

Figure 7 presents the diurnal variation of convective precipitation amount, frequency, and intensity over different sub-regions (Fig. 1) simulated with different closures. Different from the results based on total precipitation (Figs. 4, 5), the diurnal variation of convective precipitation shows relatively weak regional dependence. In the CR experiment (red curves in Fig. 7), convective precipitation peaks from noon to afternoon over all the sub-regions. In the QE experiments (blue curves in Fig. 7), convective precipitation amount generally peaks at around 1000–1200LST over all the sub-regions. Among the three closures, the QE closure simulates the largest convective precipitation amount during daytime but the smallest one during nighttime, leading to the large amplitude in precipitation diurnal change (Fig. 4d). In the FTQE experiment (green curves in Fig. 7), convective precipitation amount peaks at 1600–1700LST for all the sub-regions.

In the CR experiment, the diurnal variation of convective precipitation frequency are similar to that of convective precipitation amount, with diurnal peak from noon to afternoon when CAPE is large (shown later). By contrast, the diurnal cycle of precipitation intensity is different from that of precipitation amount or CAPE although convection intensity is strictly determined by CAPE values in the CR closure (Eq. 6). It is found that the precipitation intensity during nighttime is even stronger than that during daytime over NCP and SCB. Further inspection indicates that the stronger rainfall intensity during nighttime is due to the higher convection base at night that is

closely related to the strength of downdraft cooling (discussed later in Sect. 3.4). In the QE experiment, the diurnal phases of precipitation frequency and intensity are consistent with that of precipitation amount for all the sub-regions. In the FTQE experiment, precipitation frequency generally peaks at late afternoon. Differently, the peak time of precipitation intensity is about 3 h earlier than that of precipitation frequency.

As aforementioned, the CAPE consumption time scale τ is a key parameter for precipitation simulation when the CR closure is used (e.g. Yang et al. 2012, 2013; Qian et al. 2015). Arakawa (2004) pointed out that when τ becomes very small, the results using the CR closure would be similar to that using the QE closure. Hence, the simulated precipitation diurnal cycle could be altered by changing the value of τ in the CR closure as it determines the consumption and accumulation rates of CAPE and consequently the diurnal cycles of CAPE and precipitation.

The simulated diurnal cycle of precipitation amount in the FTQE experiment is not consistent with previous findings (e.g. Yuan 2013), which is probably because a very loose requirement is used to define the trigger function here. When the precondition of $RH > 70\%$ (see Sect. 2.2 and Table 1) is added in the trigger function, the simulated diurnal cycle of precipitation, in terms of amount, frequency, and intensity, can be altered to a large extent (Fig. 8). For the sake of brevity, only the results in eastern China (20° – 40° N and 113° – 122° E) are shown here. During daytime, convective precipitation is remarkably reduced when the RH restriction is used in all the experiments with different closures (dashed curves in Fig. 8). On the contrary, nighttime precipitation is not sensitive to the RH restriction because RH values are usually above 70% at night. When the RH restriction is included in the CR experiment, the diurnal feature of convective precipitation becomes more complicated, with two peaks of precipitation amount at late morning (1000LST) and late afternoon (1800LST). When the RH restriction is used associated with the QE closure, the peak time of convective precipitation amount is not changed although daytime precipitation is considerably reduced. In the FTQE experiment, including the RH restriction remarkably reduces the amplitude of diurnal change in convective precipitation. Figure 8b shows that the decreases in daytime precipitation are mainly because of the reduced precipitation frequency during daytime. However, daytime precipitation intensities are increased when the RH restriction is used (Fig. 8c), which is probably because weak convection is suppressed while strong convection can still occur in the model.

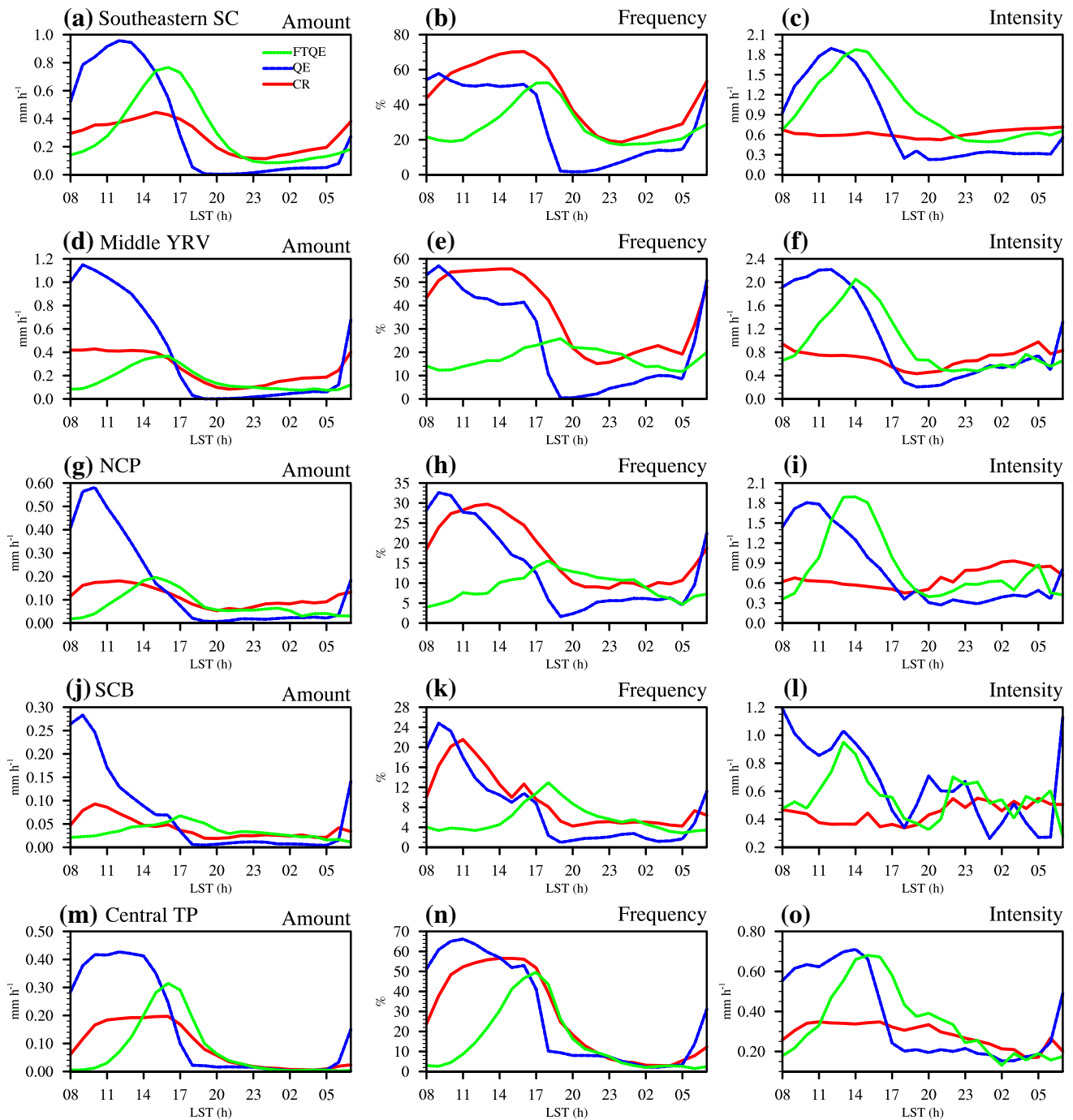


Fig. 7 Diurnal variations of convective precipitation amount (*left*), frequency (*center*), and intensity (*right*) over different sub-regions (see Fig. 1) in the summer of 2008 from the CR, QE, and FTQE simulations

3.3 Impacts of CAPE on precipitation

The convective precipitation diurnal cycle is highly correlated to the diurnal evolution of CAPE or CAPE tendency. In the QE experiment, convection intensity is determined by the change in total CAPE caused by large-scale advection, radiative, and PBL processes (Fig. 9). It is clear that

the change in total CAPE (black curve in Fig. 9) reaches its maximum value at around 1100–1400LST, corresponding to the peak time of convective precipitation amount and intensity (blue curves in Fig. 7). As Zhang (2002) stated, the change in total CAPE is mainly contributed by the PBL mixing process (red curve in Fig. 9), which is the main source of the increment in total CAPE during daytime. By

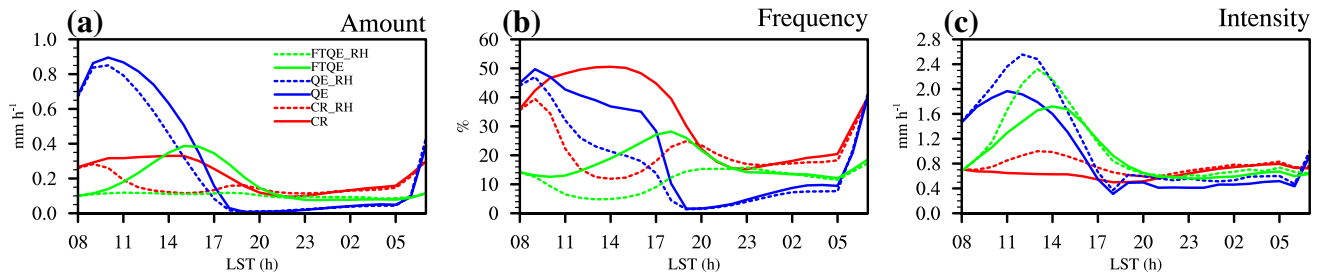


Fig. 8 Diurnal variations of convective precipitation amount (a), frequency (b), and intensity (c) over eastern China (20° – 40° N and 113° – 122° E) in the summer of 2008 from the CR/CR_RH, QE/QE_RH, and FTQE/FTQE_RH simulations

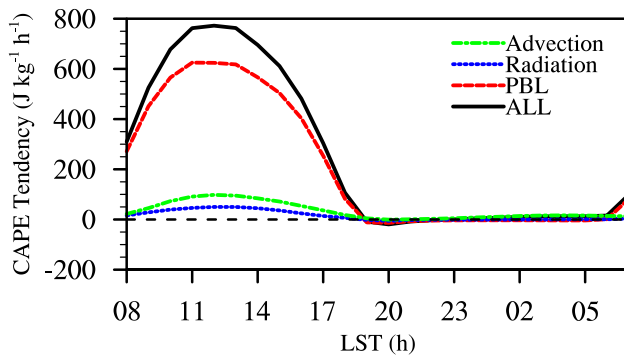


Fig. 9 Diurnal variations of CAPE tendency induced by different atmospheric processes over eastern China in the summer of 2008 from the QE simulation

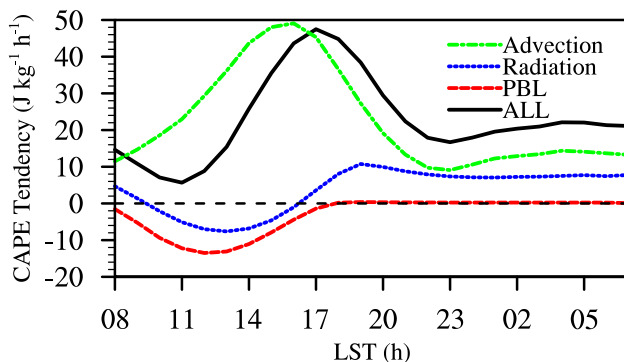


Fig. 10 Diurnal variations of CAPE tendency in the free troposphere induced by different atmospheric processes over eastern China in the summer of 2008 from the FTQE simulation

contrast, the total CAPE changes induced by advection and radiation are much weaker than that by the PBL process.

In the FTQE experiment, CAPE change due to temperature or humidity change at CSL is not used in the closure and only the changes of air properties in the free troposphere (or layers above CSL in the model) can directly affect convection intensity. As shown in Fig. 10, CAPE change due to free-troposphere processes are dominated by

advection processes (green curve in Fig. 10), which shows a diurnal peak at late afternoon. The PBL and radiation processes generally cause negative change in CAPE during daytime because they act to warm the air above CSL (figure not shown). At night, radiation process produces a positive change in CAPE because of the radiation cooling effect (figure now shown).

To better understand the impacts of different processes on the simulated convective precipitation, rainy events are classified into different categories based on their hourly rainfall amount (see Sect. 2.4, only convective precipitation amount is used for the classification). We compare the changes of total CAPE induced by different processes during events at different rain rates in the QE experiment (Fig. 11). During daytime (Fig. 11a), PBL processes play the most important role in CAPE change for all the rainy events at different rates. Advection may play some role on convection with strong intensity. During nighttime (Fig. 11b), the magnitude of CAPE change necessary for producing a strong event is much less than that during daytime. For instance, on average, the change in total CAPE reaches $6000 \text{ J kg}^{-1} \text{ h}^{-1}$ during heavy-rain events in daytime, while only about $2500 \text{ J kg}^{-1} \text{ h}^{-1}$ in nighttime. This phenomenon is related to the diurnal change in the convection base height as aforementioned and will be discussed later (Sect. 3.4). Different from the condition in daytime, large-scale advection becomes more important for the total CAPE change at night, particularly during heavy-rain events.

In the FTQE experiment (Fig. 12), stronger rainfall events are usually associated with larger changes in CAPE due to free-troposphere processes. During both daytime and nighttime, advection is the main process that determines the intensity of convection. Different from the results in QE, for a given rain category, e.g. heavy-rain events, the magnitude of CAPE change during nighttime is comparable to that during daytime. This is mainly because in the FTQE experiment, the cooling at CSL from downdraft has nearly no effect on the simulated convection intensity, and precipitation intensity is generally proportional to the

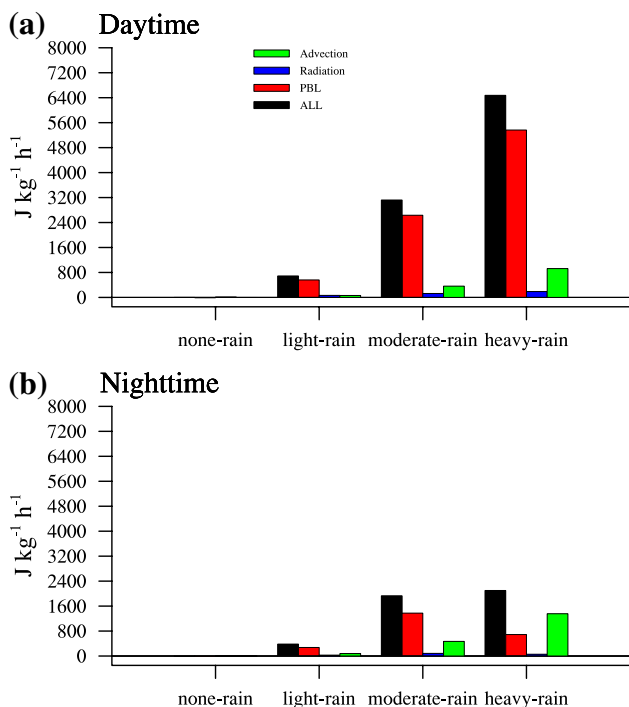


Fig. 11 CAPE tendency induced by different atmospheric processes during none-rain, light-rain, moderate-rain, and heavy-rain events in daytime (1100–1700LST; **a**) and nighttime (2300–0500LST; **b**) over eastern China in the summer of 2008 from the QE simulation

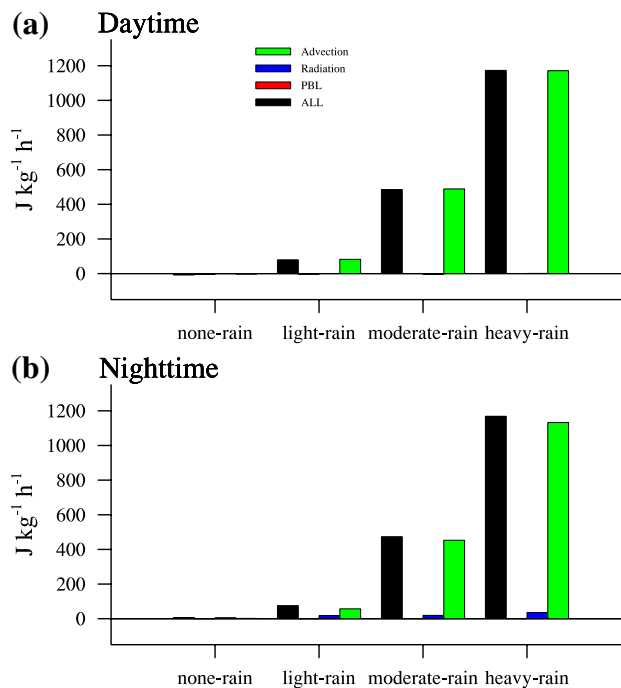


Fig. 12 Free-troposphere CAPE tendency induced by different atmospheric processes during none-rain, light-rain, moderate-rain, and heavy-rain events in daytime (1100–1700LST; **a**) and nighttime (2300–0500LST; **b**) over eastern China in the summer of 2008 from the FTQE simulation

condensation heating rate in the free troposphere, which is used to close the CPS.

In fact, different processes such as convection, PBL mixing, and advection can interact with each other so as to sustain a dynamical equilibrium in the atmosphere (Table 2). For instance, compared to the FTQE experiment, the convection-induced CAPE change in the CR or QE experiment is relatively stronger, which in turn intensifies the air mixing in the PBL. It is also found (Table 2), that in the CR experiment, CAPE change in the free-troposphere from advection is nearly balanced by that from convection (even at hourly scale, results not shown), indicating the FTQE assumption still holds though it is not used in the CR closure.

3.4 Sensitivity to model vertical resolution

Model vertical resolution particularly that in the PBL can exert large impacts on the simulated PBL properties and further affect convection (e.g. Leung et al. 1999; Cha et al. 2008). The diurnal variations of convective precipitation amounts simulated with different vertical resolutions in the PBL are compared (Fig. 13). When increasing the vertical layers in 200–2000 m, the simulated precipitation diurnal cycles are nearly unchanged in the experiments with

different closure assumptions (figure not shown). By contrast, the simulated convective precipitation is very sensitive to model vertical resolution in the lowest part of PBL (i.e. 0–200 m, see Sect. 2.2 and Table 1). When the CR closure is used, increasing the vertical layers in 0–200 m causes apparent decreases in daytime precipitation but slight increases in nighttime precipitation (red curves in Fig. 13). Compared to the low-resolution results, the peak time of precipitation over southern SC and central TP (Fig. 13a, e) is postponed by a few hours in the simulation with high resolution in 0–200 m (referred to as high-resolution simulation hereafter).

In the QE and FTQE experiments, daytime precipitation is reduced when increasing the vertical resolution in 0–200 m except for over SCB. However, the basic diurnal features such as the peak time of convective precipitation are not changed, which is different from the results in the CR experiment. It is found that the changes in precipitation amount are mainly caused by the decreases in precipitation intensity (figure not shown) rather than by the changes in precipitation frequency when high resolution is applied.

The reason responsible for the sensitivity of precipitation to model vertical resolution is further investigated based on the CR simulations. In the ZM CPS, CSL is determined as the layer with the largest CAPE in the PBL. In most

Table 2 Daily-mean CAPE tendency and free-troposphere CAPE tendency induced by different atmospheric processes over eastern China in the summer of 2008 from the CR, QE, and FTQE simulations

Experiments	CAPE tendency ($\text{J kg}^{-1} \text{h}^{-1}$)				Free-troposphere CAPE tendency ($\text{J kg}^{-1} \text{h}^{-1}$)			
	PBL	Radiation	Advection	Convection	PBL	Radiation	Advection	Convection
CR	128.4	19.1	29.6	-147.9	-2.7	3.9	32.0	-31.2
QE	207.8	14.6	33.7	-260.3	-1.7	1.0	34.1	-41.1
FTQE	86.0	22.8	18.8	-106.5	-3.2	3.6	22.5	-23.5

cases, CSL during daytime is found to be the first atmospheric layer near the surface (figure not shown). When increasing the vertical resolution in the lowest part of PBL, model layers including CSL become much thinner, leading to decrease in the height of CSL (Fig. 14a). During daytime, the height of CSL with high resolution is nearly half of that with low resolution. Decreases in the CSL height induced by increasing resolution can also be seen at night; however, the relative change is much smaller compared to that during daytime. Meanwhile, the reduced distance from CSL to surface results in an increase of CSL temperature and increase of CAPE in the high-resolution simulation (Fig. 14b). Based on the definition of the CR closure (Eq. 6), convection intensity or CAPE consumption rate by convection (Fig. 14d) is determined by CAPE values in excess of CAPE_0 . However, the responses of convective precipitation (Fig. 13) and CAPE (Fig. 14b) to increase of model resolution are not consistent with each other because of the thinner sub-cloud layer (i.e. lower CSL) in the high-resolution simulation. In fact, the detrainment of downdraft in the ZM CPS is confined to the layer below CSL, and the cooling from downdraft detrainment is uniformly added to the air mass in the sub-cloud layer. With a lower CSL height, downdrafts can induce stronger cooling at CSL (Fig. 14c) and thus the reduction in total CAPE per unit of downdraft amount is larger. As a result, compared to the low-resolution experiment, the high-resolution experiment produces less convective precipitation though the simulated CAPE and CAPE consumption rate are larger. Different from the daytime condition, the increases of CAPE could result in slight increases of nighttime precipitation as high resolution is used. Compared to the total CAPE change, the change due to convective heating in the free troposphere (Fig. 14e) agrees more with convective precipitation.

The impacts of the CSL height on the simulated precipitation can also be used to explain the sensitivity of precipitation to model vertical resolution in the QE experiments, in which the total CAPE change is used to close the equations. However, the reason responsible for the precipitation changes in the FTQE experiments is still unclear. We find that the decreases in convective precipitation are associated with the decreases in the CAPE change by free-troposphere advection when using the FTQE closure. Figure 15a shows the vertical distribution of heating rate by advection

simulated with different vertical resolutions during potential precipitating hours (i.e. with positive CAPE tendency in the free troposphere). It shows the advection cooling in the high-resolution simulation is apparent weaker than that in the low-resolution simulation. To examine whether such change of advection cooling is caused by feedbacks of convection or by other processes, we also show the profiles of advection cooling in simulations with convection turned off (Fig. 15b). We find, that in the non-convection simulations, the sensitivity of advection cooling to model vertical resolution is not as clear as that in the FTQE simulations. Thus, the feedback of convection on the free-troposphere advection should be considered when studying the impacts of PBL resolution on precipitation. As discussed above, model vertical resolution in the PBL can affect the CAPE calculation. Although the total CAPE value is not used in the FTQE closure, it can affect the vertical extension of updraft motion and thus the vertical profile of convective heating, which may further influence the closure of convection. However, further investigation with additional experiments are needed to better understand this phenomenon, which is beyond the scope of this study.

As aforementioned, convective precipitation intensity during nighttime may exceed that during daytime in the CR experiments (red curves in Fig. 7) although the CAPE values are much larger in daytime. Increasing the PBL vertical resolution can further enhance the nighttime precipitation but decrease the daytime precipitation. In fact, the strong nighttime precipitation is also related to the diurnal change in the CSL height. After sunset, CSL is gradually lifted from near the surface to upper layers (Fig. 14a), which leads to increases in the thickness of sub-cloud layer and decreases in the downdraft cooling. As a result, the PBL properties and thus the total CAPE are less affected by downdraft, indicating that a relatively strong updraft associated with strong precipitation intensity is needed to efficiently remove CAPE during nighttime.

4 Summary and discussion

We evaluated the precipitation diurnal cycles over East Asia during the summer of 2008 simulated with three different CAPE-based convective closure assumptions in

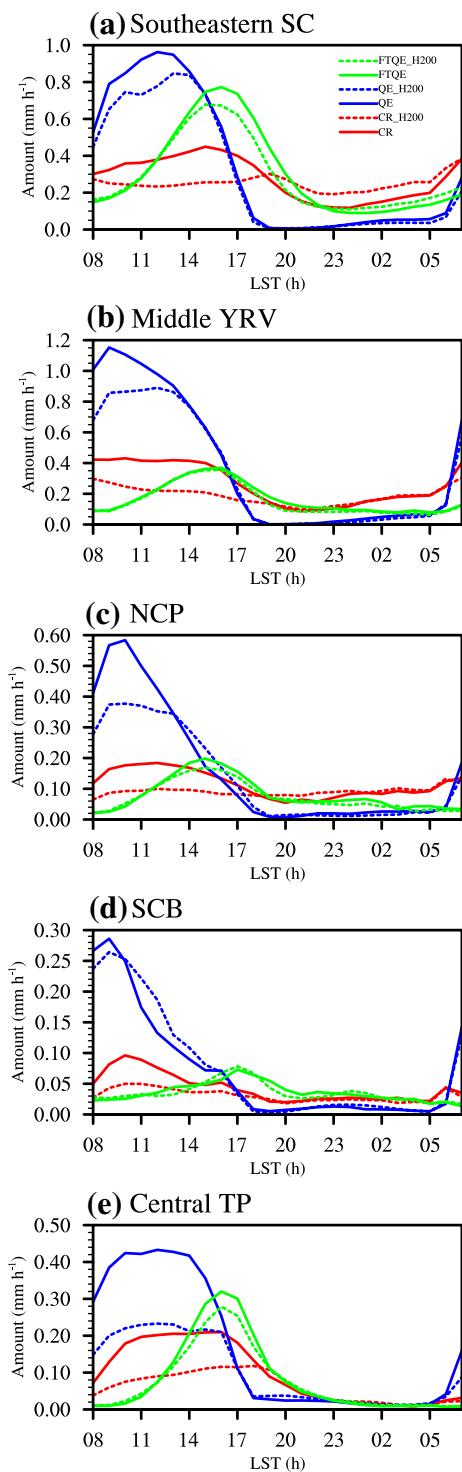


Fig. 13 Diurnal variations of convective precipitation amount over different sub-regions (see Fig. 1) in the summer of 2008 from the CR/CR_H200, QE/QE_H200, and FTQE/FTQE_H200 simulations

WRF. Simulations with different vertical resolutions within the PBL were conducted for each closure to explore the potential impacts of vertical resolution on the precipitation diurnal cycle. Results show that the differences in

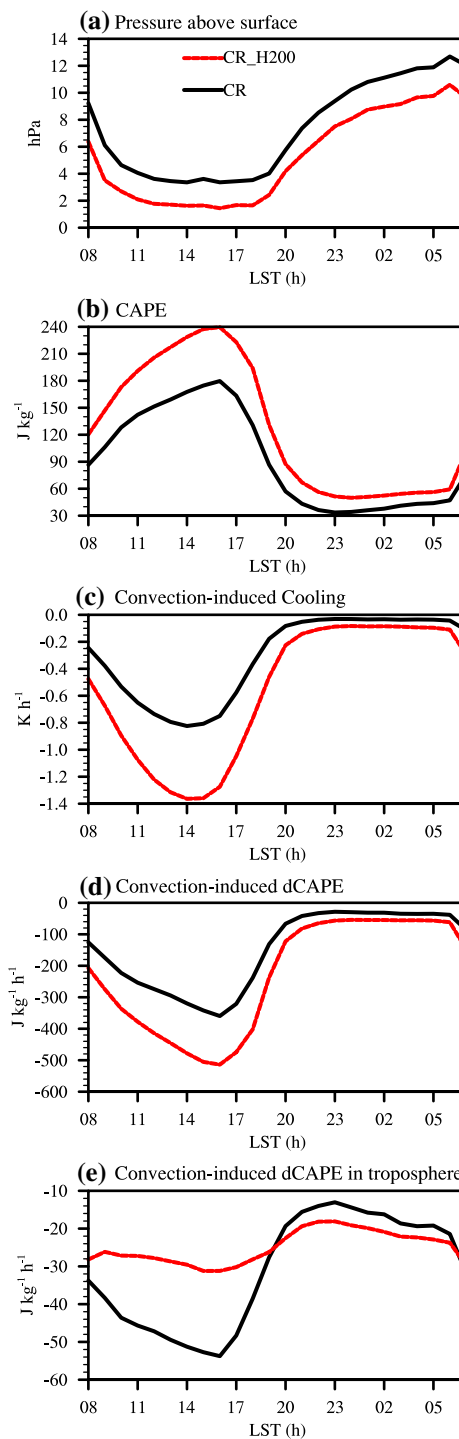


Fig. 14 Diurnal variations of pressure above surface at CSL (a), CAPE (b), convection-induced cooling near the surface (c), CAPE tendency (d), and free-troposphere CAPE tendency (e) over eastern China in the summer of 2008 from the CR and CR_H200 simulations

precipitation diurnal phases among different experiments are more apparent over land than over ocean regions. The simulated precipitation generally peaks at early morning over oceans, particularly over the near-land areas, which

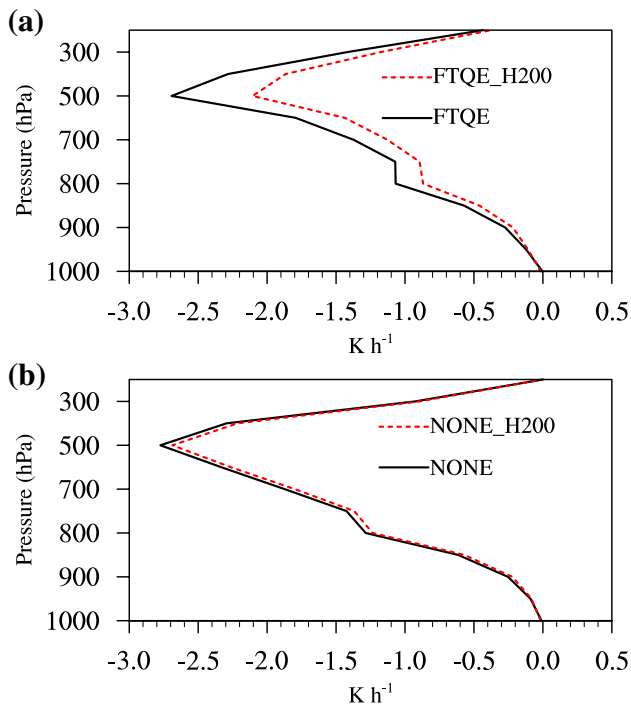


Fig. 15 Vertical profiles of heating induced by advection during potential precipitating hours in daytime (1100–1700LST) over eastern China in the summer of 2008 from the FTQE/FTQE_H200 (a) and NONE/NONE_H200 (b) simulations

is overall consistent with the TRMM observation. On the contrary, all the experiments have difficulties in realistically reproducing the diurnal variation of precipitation over land. Compared to the CR and QE closures, the simulation with FTQE closure shows better agreements with observation in terms of precipitation diurnal cycle, such as the nocturnal precipitation over SCB. The better simulated precipitation diurnal phases by the FTQE closure are likely because of the reasonable partitioning between convective and stratiform precipitation.

The diurnal phases of convective precipitation simulated by different closures were compared in detail. In the simulation with CR closure, convective precipitation amount generally peaks at afternoon, associating with the afternoon peak of precipitation frequency. In the simulation with QE closure, convective precipitation amount peaks at late morning as the PBL mixing is gradually intensified after sunrise; however, advection process also contributes to the development of strong convection events, particularly during nighttime. In the simulation with FTQE closure, the diurnal cycle of convective precipitation is mainly determined by the CAPE change from advection cooling in the free troposphere. In fact, different atmospheric processes can be affected by each other at diurnal scale and thereby, the dynamical equilibrium in the free troposphere can still be reached in the simulation with CR closure, implying the

complex cause-effect relationship between atmospheric motion and convection.

Further sensitivity results show that increasing the number of vertical layers in the lowest part of PBL results in reduction of daytime precipitation in the simulations with CR and QE closures, which is because higher vertical resolution causes lower CSL height that leads to stronger downdraft cooling and CAPE consumption during daytime. For some regions (Fig. 13), the precipitation diurnal peak in the CR simulation occurs earlier than in the FTQE simulation as low resolution is used, but occurs later as high resolution is used; thereby, the impacts of closure assumption on precipitation simulation could be modulated by other model configurations such as the vertical resolution in the PBL. The impacts of the CSL height can also explain the stronger precipitation intensity in nighttime than daytime over some regions in the CR simulation, i.e. the lifting of CSL after sunset causes decrease of CAPE consumption rate, and thus a relatively small value of CAPE is needed to produce a strong convection event. These results indicate, that in convective closures based on the total CAPE value, factors related to downdraft properties can remarkably affect the simulated precipitation diurnal cycle.

Analyses presented here were based on WRF simulations that were reinitiated every day, which can prevent the free growth of bias in large-scale circulation but allow processes at diurnal or sub-diurnal scale, such as the interaction between the PBL and free-troposphere atmosphere, to take place. Hence, this study helps better understand the impacts of various atmospheric processes (i.e. PBL mixing and advection/radiation heating or cooling) and dynamical configurations in the PBL on the precipitation diurnal cycles simulated with different convective closures but meanwhile with the inter-simulation differences in large-scale circulations minimized. However, free-run simulations with GCMs are needed to further quantify the feedbacks of convection on large-scale circulation when different closures are applied. In the future, we also intend to evaluate the simulated precipitation diurnal cycles using closures based on moisture advection and air vertical motion over East Asia. In addition, many other processes such as updraft, downdraft, entrainment, and cloud-precipitation conversion can have large impacts on the generation of precipitation (e.g. Zhang 2009; Wu 2012; Yang et al. 2012, 2015b; Qian et al. 2015). For instance, compared to the ZM scheme, the source layer of updraft in the Kain–Fritsch scheme is defined as a mixture of vertically adjacent layers that is at least 60 hPa thick (Kain 2004), which potentially makes the updraft/downdraft characteristics more stable and thus reduces the sensitivity of simulated precipitation to model vertical resolution, particularly as the total CAPE value is used for the closure. Therefore, the impacts of

different processes in convection system and their interactions on the simulated precipitation diurnal variation deserve further investigations.

Acknowledgements We thank two anonymous reviewers for their careful reviews and constructive comments. We also thank Minghui Wang of Nanjing University for his valuable discussions and Jian Tang of China Meteorological Administration for processing the station rain-gauge data. This work is jointly supported by the National Natural Science Foundation of China (41675101 and 41305084) and National key research and development program (2016YFA0602104 and 2016YFA0600504). The contribution of Yun Qian in this study is supported by the U.S. Department of Energy's Office of Science as part of the Atmospheric System Research (ASR) program. The Pacific Northwest National Laboratory is operated for DOE by Battelle Memorial Institute under contract DE-AC05-76RL01830. All the graphics in this study are created by the NCAR Command Language (NCL; doi:10.5065/D6WD3XH5).

References

- Arakawa A (2004) The cumulus parameterization problem: past, present, and future. *J Clim* 17:2493–2525
- Arakawa A, Schubert WH (1974) Interaction of a cumulus cloud ensemble with large-scale environment, part I. *J Atmos Sci* 31:674–701
- Bao Q, Lin PF, Zhou TJ, Liu YM, Yu YQ, Wu GX, He B, He J, Li LJ, Li JD, Li YC, Liu HL, Qiao FL, Song ZY, Wang B, Wang J, Wang PF, Wang XC, Wang ZZ, Wu B, Wu TW, Xu YF, Yu HY, Zhao W, Zheng WP, Zhou LJ (2013) The flexible global ocean-atmosphere-land system model, spectral version 2: FGOALS-s2. *Adv Atmos Sci* 30:561–576. doi:10.1007/s00376-012-2113-9
- Barker HW, Pincus R, Morcrette J-J (2003) The Monte-Carlo independent column approximation: application within largescale models. In: Proceedings of the GCSS/ARM Workshop on the Representation of Cloud Systems in Large-Scale Models, May 2002, Kananaskis, Alberta, Canada, p 10
- Bechtold P, Semane N, Lopez P, Chaboureaud J-P, Beljaars A, Bormann N (2014) Representing equilibrium and nonequilibrium convection in large-scale models. *J Atmos Sci* 71:734–753. doi:10.1175/jas-d-13-0163.1
- Bretherton CS, Park S (2009) A new moist turbulence parameterization in the community atmosphere model. *J Clim* 22:3422–3448. doi:10.1175/2008jcli2556.1
- Brown JM (1979) Mesoscale unsaturated downdrafts driven by rainfall evaporation: numerical study. *J Atmos Sci* 36:313–338. doi:10.1175/1520-0469(1979)036<0313:Muddbr>2.0.Co;2
- Cha DH, Lee DK, Hong SY (2008) Impact of boundary layer processes on seasonal simulation of the East Asian summer monsoon using a Regional Climate Model. *Meteorol Atmos Phys* 100:53–72. doi:10.1007/s00703-008-0295-6
- Chen F, Dudhia J (2001) Coupling an advanced land surface-hydrology model with the Penn State-NCAR MM5 modeling system. Part I: model implementation and sensitivity. *Mon Weather Rev* 129:569–585
- Chen S et al (2016) Precipitation spectra analysis over china with high-resolution measurements from optimally-merged satellite/gauge observations-part II: diurnal variability analysis. *IEEE J Stars* 9:2979–2988. doi:10.1109/JSTARS.2016.2529001
- Dai A (1999) Recent changes in the diurnal cycle of precipitation over the United States. *Geophys Res Lett* 26:341–344. doi:10.1029/1998gl900318
- Dai A, Trenberth KE (2004) The diurnal cycle and its depiction in the Community Climate System Model. *J Clim* 17:930–951. doi:10.1175/1520-0442(2004)017<0930:Tdcaid>2.0.Co;2
- Donner LJ, Phillips VT (2003) Boundary layer control on convective available potential energy: implications for cumulus parameterization. *J Geophys Res*. doi:10.1029/2003jd003773
- Emanuel KA (1995) The behavior of a simple hurricane model using a convective scheme based on subcloud-layer entropy equilibrium. *J Atmos Sci* 52:3960–3968. doi:10.1175/1520-0469(1995)052<3960:Tboash>2.0.Co;2
- Frank WM, Cohen C (1987) Simulation of tropical convective systems 0.1. A cumulus parameterization. *J Atmos Sci* 44:3787–3799. doi:10.1175/1520-0469(1987)044<3787:Sotcsp>2.0.Co;2
- Grell GA (1993) Prognostic evaluation of assumptions used by cumulus parameterizations. *Mon Weather Rev* 121:764–787. doi:10.1175/1520-0493(1993)121<0764:Peoaub>2.0.Co;2
- He HZ, Zhang FQ (2010) Diurnal variations of warm-season precipitation over Northern China. *Mon Weather Rev* 138:1017–1025. doi:10.1175/2010MWR3356.1
- Huang A, Zhao Y, Zhou Y, Yang B, Zhang L, Dong X, Fang D, Wu Y (2016) Evaluation of multisatellite precipitation products by use of ground-based data over China. *J Geophys Res Atmos* 121:10654–10675. doi:10.1002/2016jd025456
- Huffman GJ, Adler RF, Morrissey MM, Bolvin DT, Curtis S, Joyce R, McGavock B, Susskind J (2001) Global precipitation at one-degree daily resolution from multisatellite observations. *J Hydrometeorol* 2:36–50
- Huffman GJ, Adler RF, Bolvin DT, Gu GJ, Nelkin EJ, Bowman KP, Hong Y, Stocker EF, Wolff DB (2007) The TRMM multisatellite precipitation analysis (TMPA): Quasi-global, multiyear, combined-sensor precipitation estimates at fine scales. *J Hydrometeorol* 8:38–55. doi:10.1175/Jhm560.1
- Janjić ZI (1994) The step-mountain eta coordinate model—further developments of the convection, viscous sublayer, and turbulence closure schemes. *Mon Weather Rev* 122:927–945
- Janjić ZI (2002) Nonsingular implementation of the Mellor–Yamada level 2.5 scheme in the NCEP Meso model. NCEP office note 437:61
- Ji D, Wang L, Feng J, Wu Q, Cheng H, Zhang Q, Yang J, Dong W, Dai Y, Gong D, Zhang RH, Wang X, Liu J, Moore JC, Chen D, Zhou M (2014) Description and basic evaluation of Beijing Normal University Earth System Model (BNU-ESM) version 1. *Geosci Model Dev* 7:2039–2064. doi:10.5194/gmd-7-2039-2014
- Jin EK, Choi I-J, Kim S-Y, Han J-Y (2016) Impact of model resolution on the simulation of diurnal variations of precipitation over East Asia. *J Geophys Res Atmos* 121:1652–1670. doi:10.1002/2015jd023948
- Kain JS (2004) The Kain–Fritsch convective parameterization: an update. *J Appl Meteorol* 43:170–181
- Kain JS, Fritsch JM (1993) Convective parameterization for mesoscale models: the Kain–Fritsch scheme. In: Emanuel KA, Raymond DJ (eds) The representation of cumulus convection in numerical models. American Meteorology Society, Boston, p 246
- Kozu T, Kawanishi T, Kuroiwa H, Kojima M, Oikawa K, Kumagai H, Okamoto K, Okumua M, Nakatsuka H, Nishikawa K (2001) Development of precipitation radar onboard the Tropical Rainfall Measuring Mission (TRMM) satellite. *IEEE Trans Geosci Remote* 39:102–116
- Krishnamurti TN, Lownam S, Pasch R (1983) Cumulus parameterization and rainfall rates II. *Mon Weather Rev* 111:815–828. doi:10.1175/1520-0493(1983)111<0815:Cparri>2.0.Co;2
- Lee MI, Schubert SD, Suarez MJ, Schemm J-KE, Pan H-L, Han J, Yoo S-H (2008) Role of convection triggers in the simulation of the diurnal cycle of precipitation over the United States

- Great Plains in a general circulation model. *J Geophys Res.* doi:10.1029/2007jd008984
- Leung LR, Ghan SJ, Zhao ZC, Luo Y, Wang WC, Wei HL (1999) Intercomparison of regional climate simulations of the 1991 summer monsoon in eastern Asia. *J Geophys Res* 104:6425–6454. doi:10.1029/1998jd200016
- Li J, Yu RC, Zhou TJ (2008) Seasonal variation of the diurnal cycle of rainfall in southern contiguous China. *J Clim* 21:6036–6043. doi:10.1175/2008JCLI2188.1
- Liang XZ, Li L, Dai A, Kunkel KE (2004) Regional climate model simulation of summer precipitation diurnal cycle over the United States. *Geophys Res Lett* 31:L24208. doi:10.1029/2004GL021054
- Ma PL, Rasch PJ, Fast JD, Easter RC, Gustafson WI Jr, Liu X, Ghan SJ, Singh B (2014) Assessing the CAM5 physics suite in the WRF-Chem model: implementation, resolution sensitivity, and a first evaluation for a regional case study. *Geosci Model Dev* 7:755–778. doi:10.5194/gmd-7-755-2014
- Morrison H, Curry JA, Khvorostyanov VI (2005) A new double-moment microphysics parameterization for application in cloud and climate models. Part I: description. *J Atmos Sci* 62:1665–1677
- Neale RB, Richter JH, Jochum M (2008) The impact of convection on ENSO: from a delayed oscillator to a series of events. *J Clim* 21:5904–5924. doi:10.1175/2008jcli2244.1
- Park S, Bretherton CS (2009) The University of Washington shallow convection and moist turbulence schemes and their impact on climate simulations with the community atmosphere model. *J Clim* 22:3449–3469. doi:10.1175/2008jcli2557.1
- Pincus R, Barker HW, Morcrette JJ (2003) A fast, flexible, approximate technique for computing radiative transfer in inhomogeneous cloud fields. *J Geophys Res* 108:4376. doi:10.1029/2002JD003322
- Qian Y, Leung LR (2007) A long-term regional simulation and observations of the hydroclimate in China. *J Geophys Res* 112:D14104. doi:10.1029/2006jd008134
- Qian Y, Yan H, Hou Z, Johannesson G, Klein S, Lucas D, Neale R, Rasch P, Swiler L, Tannahill J, Wang H, Wang M, Zhao C (2015) Parametric sensitivity analysis of precipitation at global and local scales in the Community Atmosphere Model CAM5. *J Adv Model Earth Syst* 7:382–411. doi:10.1002/2014ms000354
- Qiao FX, Liang XZ (2015) Effects of cumulus parameterizations on predictions of summer flood in the Central United States. *Clim Dyn* 45:727–744. doi:10.1007/s00382-014-2301-7
- Qiao FX, Liang XZ (2016) Effects of cumulus parameterization closures on simulations of summer precipitation over the United States coastal oceans. *J Adv Model Earth Syst* 8:764–785. doi:10.1002/2015MS000621
- Raymond DJ (1995) Regulation of moist convection over the West Pacific warm pool. *J Atmos Sci* 52:3945–3959. doi:10.1175/1520-0469(1995)052<3945:Romcot>2.0.Co;2
- Schumacher C, Houze RA (2003) Stratiform rain in the tropics as seen by the TRMM precipitation radar. *J Clim* 16:1739–1756
- Skamarock WC, Klemp JB, Dudhia J, Gill DO, Barker DM, Duda MG, Huang X-Y, Wang W, Powers JG (2008) A description of the advanced research WRF Version 3. NCAR Technical Note, NCAR/TN-475+STR
- Suhas E, Zhang GJ (2014) Evaluation of trigger functions for convective parameterization schemes using observations. *J Clim* 27:7647–7666. doi:10.1175/jcli-d-13-00718.1
- Suhas E, Zhang GJ (2015) Evaluating convective parameterization closures using cloud-resolving model simulation of tropical deep convection. *J Geophys Res Atmos* 120:1260–1277. doi:10.1002/2014jd022246
- Wu TW (2012) A mass-flux cumulus parameterization scheme for large-scale models: description and test with observations. *Clim Dyn* 38:725–744. doi:10.1007/s00382-011-0995-3
- Wu TW, Yu RC, Zhang F, Wang ZZ, Dong M, Wang LN, Jin X, Chen DL, Li L (2010) The Beijing Climate Center atmospheric general circulation model: description and its performance for the present-day climate. *Clim Dyn* 34:123–147. doi:10.1007/s00382-008-0487-2
- Wu CM, Lo MH, Chen WT, Lu CT (2015) The impacts of heterogeneous land surface fluxes on the diurnal cycle precipitation: a framework for improving the GCM representation of land–atmosphere interactions. *J Geophys Res* 120:3714–3727. doi:10.1002/2014JD023030
- Yang B, Qian Y, Lin G, Leung LR, Zhang Y (2012) Some issues in uncertainty quantification and parameter tuning: a case study of convective parameterization scheme in the WRF regional climate model. *Atmos Chem Phys* 12:2409–2427. doi:10.5194/acp-12-2409-2012
- Yang B, Qian Y, Lin G, Leung LR, Rasch PJ, Zhang GJ, McFarlane SA, Zhao C, Zhang Y, Wang H, Wang M, Liu X (2013) Uncertainty quantification and parameter tuning in the CAM5 Zhang–McFarlane convection scheme and impact of improved convection on the global circulation and climate. *J Geophys Res Atmos* 118:395–415. doi:10.1029/2012jd018213
- Yang B, Zhang Y, Qian Y, Huang A, Yan H (2015a) Calibration of a convective parameterization scheme in the WRF model and its impact on the simulation of East Asian summer monsoon precipitation. *Clim Dyn* 44:1661–1684. doi:10.1007/s00382-014-2118-4
- Yang B, Zhang Y, Qian Y, Wu T, Huang A, Fang Y (2015b) Parametric sensitivity analysis for the Asian summer monsoon precipitation simulation in the Beijing climate center AGCM, Version 2.1. *J Clim* 28:5622–5644. doi:10.1175/jcli-d-14-00655.1
- Yano JI, Bister M, Fuchs Ž, Gerard L, Phillips VTJ, Barkidija S, Piriou JM (2013) Phenomenology of convection-parameterization closure. *Atmos Chem Phys* 13:4111–4131. doi:10.5194/acp-13-4111-2013
- Yu RC, Zhou TJ, Xiong AY, Zhu YJ, Li JM (2007) Diurnal variations of summer precipitation over contiguous China. *Geophys Res Lett* 34:L01704. doi:10.1029/2006gl028129
- Yuan W (2013) Diurnal cycles of precipitation over subtropical China in IPCC AR5 AMIP simulations. *Adv Atmos Sci* 30:1679–1694. doi:10.1007/s00376-013-2250-9
- Yuan W, Yu R, Li J (2013) Changes in the diurnal cycles of precipitation over eastern China in the past 40 years. *Adv Atmos Sci* 30:461–467. doi:10.1007/s00376-012-2092-x
- Zhang GJ (2002) Convective quasi-equilibrium in midlatitude continental environment and its effect on convective parameterization. *J Geophys Res.* doi:10.1029/2001jd001005
- Zhang GJ (2009) Effects of entrainment on convective available potential energy and closure assumptions in convection parameterization. *J Geophys Res* 114:D07109. doi:10.1029/2008jd010976
- Zhang Y, Chen H (2016) Comparing CAM5 and superparameterized CAM5 simulations of summer precipitation characteristics over continental East Asia: mean state, frequency–intensity relationship, diurnal cycle, and influencing factors. *J Clim* 29:1067–1089. doi:10.1175/jcli-d-15-0342.1
- Zhang GJ, McFarlane NA (1995) Sensitivity of climate simulations to the parameterization of cumulus convection in the Canadian climate center general-circulation model. *Atmos Ocean* 33:407–446
- Zhou TJ, Yu RC, Chen HM, Dai A, Pan Y (2008) Summer precipitation frequency, intensity, and diurnal cycle over China: a comparison of satellite data with rain gauge observations. *J Clim* 21:3997–4010. doi:10.1175/2008JCLI2028.1